Thin-plate modeling of interseismic deformation and asymmetry across the Altyn Tagh fault zone

R. Jolivet,[1] R. Cattin,[1] N. Chamot-Rooke,[1] C. Lasserre,[1] and G. Peltzer[2,3]

Received 30 July 2007; revised 13 October 2007; accepted 6 December 2007; published 30 January 2008.

[1] Creeping dislocations in an elastic half-space are commonly used to model interseismic deformation. However, this semi-infinite conventional model can lead to biased inferences of the slip rate and the fault locking depth. We therefore favor the use of a thin-plate model sheared at its base in agreement with the current knowledge of the seismogenic thickness of the lithosphere. We apply these two approaches to interpret InSAR data across the Altyn Tagh fault system near longitude 94°E, in a region of clear asymmetry of interseismic velocity distribution. Our results suggest a locking depth of 7–9 km and a present-day geodetic slip rate of 8–10 mm/yr, consistent with the rate based on GPS measurements at this longitude. We interpret the asymmetric pattern as the joint effect of a rigidity decrease from the Tarim basin north of the fault to the Qaidam basin south of it and of a 5–7 km southward offset of strain concentration from the quaternary northern active fault. This suggests that the rigidity contrast as well as most of the creep at depth occurs on the southern geological fault.
Citation: Jolivet, R., R. Cattin, N. Chamot-Rooke, C. Lasserre, and G. Peltzer (2008), Thin-plate modeling of interseismic deformation and asymmetry across the Altyn Tagh fault zone, *Geophys. Res. Lett.*, *35*, L02309, doi:10.1029/2007GL031511.

1. Introduction

[2] Creeping dislocations buried in an elastic homogeneous half-space are commonly used to explain geodetic observations across active faults [e.g., *Vergne et al.*, 2001; *Smith and Sandwell*, 2003; *Wang et al.*, 2003]. This modeling provides an estimate of both the slip rate of the fault and its locking depth, which can be used to quantify interseismic strain accumulation at depth.

[3] Over the last two decades, dense and continuous GPS and EDM networks, creepmeter measurements as well as InSAR data have provided a high spatial coverage and accurate measurements of interseismic deformation across major continental strike-slip faults [e.g., *Sieh and Williams*, 1990; *Wright and Fielding*, 2001; *Fialko*, 2006]. These high-quality data have revealed significant deviations from predictions of elastic dislocation models, particularly asymmetric patterns of interseismic velocities across these faults such as the San Andreas fault [*Savage et al.*, 2004] or the North Anatolian fault [*Meade et al.*, 2002].

[4] The interpretation of such deviations requires improvements of standard elastic dislocation models used to simulate interseismic velocities. Here, we propose a new modeling approach, which includes a finite thickness of the elastic plate, a shear zone beneath the locked fault and a rigidity contrast on both sides of the fault. We first describe the modeling approach and assumptions and compare both approaches for vertical strike-slip faults, by studying the relationship between the locking depth used in elastic dislocation models and the thickness of the elastic plate in our modeling. We next introduce asymmetric geometry and material properties in the model and compare the results to the eastern section of the Altyn Tagh Fault at longitude 94°E where interseismic GPS and InSAR displacements are now available [*Lasserre et al.*, 2007; *Zhang et al.*, 2007].

2. Modeling Approaches and Assumptions

2.1. Elastic Half-Space

[5] Interseismic velocities near a vertical strike-slip fault creeping below a depth D are commonly calculated from a model based on a screw dislocation buried in an homogeneous elastic half-space [*Chinnery*, 1961; *Savage and Burford*, 1973]

$$V(x) = \frac{V_T}{\pi}\arctan\left(\frac{x}{D}\right), \tag{1}$$

where V is the fault-parallel velocity, x the distance from the fault, D the locking depth and V_T the far-field velocity, usually associated with the long-term slip rate. In this analytic model (herein after HSM for Half-Space Model), an infinitely long dislocation is required to simulate far-field velocity (Figure 1a).

2.2. Elastic Thin-Plate

[6] For major strike-slip faults, including the San Andreas Fault, the North Anatolian Fault or the Sumatra Fault, the depth distribution of earthquakes and the estimated locking depth suggest that the bottom of the elastic layer in the lithosphere most often lies between 10 and 15 km and does not exceed ~25 km [e.g., *Smith and Sandwell*, 2003; *Le Pichon et al.*, 2005]. This small elastic thickness is not consistent with the assumption of a semi-infinite elastic media, which is used in the half-space model (Figure 1a). An alternative approach is to use a finite thickness for the elastic part of the lithosphere (Figure 1b). In this model (herein after TPM for Thin-Plate Model), we prescribe a constant velocity on both sides of the fault at the base of a thin elastic plate. Following *Pollitz and Nyst* [2005], we assume a weak lithosphere. We distinguish the elastic upper

[1]UMR 8538, Laboratoire de Géologie, ENS, CNRS, Paris, France.
[2]Department of Earth and Space Sciences, University of California, Los Angeles, California, USA.
[3]Jet Propulsion Laboratory, California Institute of Technology, Pasadena, USA.

0094-8276/08/2007GL031511$05.00

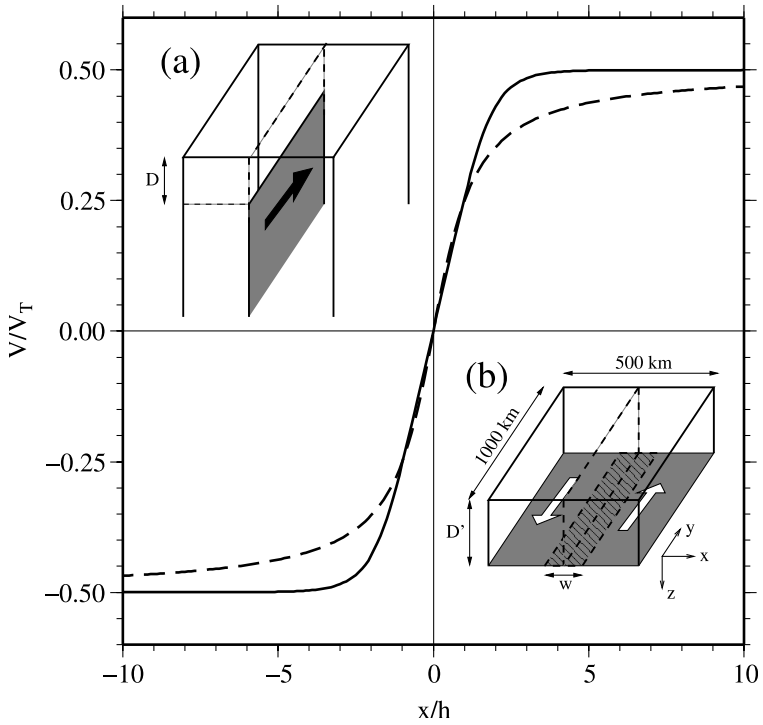

Figure 1. Normalized surface velocity across a vertical strike-slip fault calculated with the half-space model (dashed line) and the thin-plate model (solid line). x is the distance from the fault. h is equal to D or D' for the half-space model and thin-plate model, respectively. (a) Geometry of the half-space model. Vertical dislocation with a Burgers's vector increasing at a rate of V_T. D is the locking depth of seismogenic fault zone. (b) Geometry and boundary conditions of the thin-plate model. A strike slip velocity of $V_T/2$ is imposed at the base of the model (white arrow). D' is the thickness of the elastic plate. w is the width of a transition zone between the two opposite velocities imposed at the base of the model.

part of the crust, where interseismic stress is located, from the lower part, which behaves as a fluid at the time scale of interseimic deformation. We assume the fault to be locked over the entire thickness D' of the elastic layer (Figure 1b).

[7] Simulations are performed using the three-dimensional finite element code ADELI [*Chéry et al.*, 2001]. We consider two elastic plates with their own rigidity on each side of a fault, with a locked interface to simulate interseismic motion. To reduce edge effects, we consider a plate with horizontal dimension of 500 km and 1000 km in the across-fault and along-fault directions, respectively. Elements size is 5 km throughout the model and decreases around the fault to allow for a better description of the strain there. At the vertical borders, both vertical and along-fault velocities are free. We apply shear under the plate by fixing an opposite velocity $V_T/2$ at the base of the model on both sides of the fault. A transition zone of width w centered at the fault between these two domains remains free. We test the effect of the width of this zone for w/D' ranging between 0 and 10 (see Figure S1 in auxiliary material[1]). Change in w has no significant effect on the calculated surface displacements for $w/D' < 1.5$. This ratio is consistent with the estimated width of the strongly foliated and lineated mylonitic gneissic zones described by *Leloup et al.* [1995] along the Ailao Shan–Red River shear zone. In the following, we thus arbitrarily set $w/D' = 1$.

2.3. Comparison Between Half-Space Model and Thin-Plate Model

[8] To compare the HSM and TPM models, we calculate surface velocities for a Young's modulus $E = 100$ GPa and a Poisson's ratio $v = 0.25$ on both sides of the fault. Assuming that $D = D'$, Figure 1 shows that both models give consistent velocities nearby the fault ($|x| < D$). However, in the far-field the shape of the velocity profiles are very different. In the case of the half-space model, the far-field velocity is reached only for $|x| > 10\ D$. In the case of a thin-plate model, the far-field velocity is reached at a distance as small as $\sim 3D'$.

[9] This difference in the surface velocity profiles is related to the distribution of the deformation at depth. Implicit in the half-space model is that part of the elastic deformation is stored below the locking depth. This leads to distributed deformation at distances up to 10 D from the fault (see Figure S2 of auxiliary material). In the thin-plate model, there is no elastic stress stored below the depth D', resulting in elastic shear strain being concentrated closer to the fault at the surface.

[10] This result emphasizes the importance of the HSM assumptions commonly used to model interseismic displacement. To quantify the locking depth estimate bias between the two models, we adjust the HSM parameters

[1] Auxiliary materials are available in the HTML. doi:10.1029/2007GL031511.

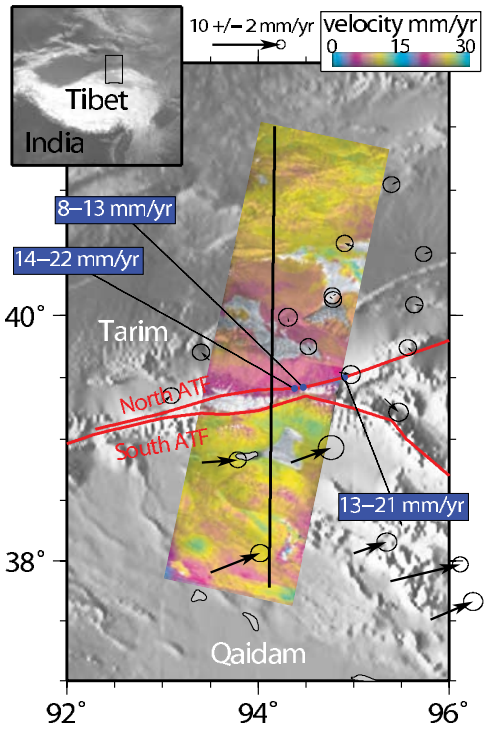

Figure 2. Map of the Altyn Tagh fault system. Holocene estimates of the slip rate along the Altyn Tagh fault is given in blue boxes [*Van der Woerd et al.*, 2001; *Mériaux et al.*, 2005; *Zhang et al.*, 2007]. Black arrows represent GPS velocities [*Zhang et al.*, 2007]. Colored area shows surface velocity (projected in fault-parallel direction) obtained from a stack of 15 interferograms using ERS and ENVISAT radar data covering the 1995–2006 period [*Lasserre et al.*, 2007]. Solid line is location of profile shown in Figure 3.

to velocity profiles computed with the TPM for D' varying between 5 and 50 km. The results indicate that $D \sim 0.65D'$ over the explored range.

[11] As previously mentioned by *Savage* [2006], this result suggests that the use of a half-space model to interpret interseismic velocity fields leads to underestimate the fault locking depth or to overestimate its slip rate if the far-field velocity is not well-constrained by geodetic data.

2.4. Asymmetric Model

[12] Possible explanations of asymmetry in interseismic velocities with respect to surface traces of strike-slip faults include horizontal offset between the fault trace and the creeping zone due to a non-vertical fault geometry at the surface or deeper, post-seismic relaxation with lateral variations in crustal viscosity and rigidity contrast on both sides of the faults [e.g., *Le Pichon et al.*, 2005; *Schmalzle et al.*, 2006; *Fialko*, 2006]. In the next section we apply our model to the eastern Altyn Tagh fault assuming a single vertical fault and no major earthquake over the last century. The simplest parametrization to account for asymmetry reduces to two parameters: the rigidity contrast between the two sides of the fault and the horizontal offset between the basal shear zone and the surface fault.

[13] Following *Le Pichon et al.* [2003], we modified the half-space model to calculate an asymmetric surface velocity field on each side of the fault

$$V(x) = \begin{cases} \dfrac{2KV_T}{\pi}\arctan\left(\dfrac{x-\Delta}{D}\right) & \text{if } x > \Delta \\ \dfrac{2(1-K)V_T}{\pi}\arctan\left(\dfrac{x-\Delta}{D}\right) & \text{if } x < \Delta \end{cases} \quad (2)$$

where D is the locking depth, x the distance from the surface fault trace, Δ the horizontal offset between this fault trace and the buried dislocation, and V_T the far-field velocity. The asymmetry coefficient $K = V_1/(V_1 + V_2) = V_1/V_T$ ranges from 0 to 1. This coefficient can also be written in terms of rigidity ratio $E_2/(E_1 + E_2)$. The equations 1 and 2 are equivalent for $\Delta = 0$ (no dislocation offset) and $K = 0.5$ (no rigidity contrast).

[14] By shifting the calculated velocity curves, the apparent velocity ratio V_1/V_T changes, because the surface trace of the fault is fixed, while the rheology ratio $E_1/(E_1 + E_2)$ keeps constant. This shows the trade-off between lateral variations in rocks rheology and the offset between the fault trace and the buried creeping zone.

[15] An alternative approach is to use an asymmetric thin-plate model in which the far field velocity is fixed on both sides of the fault independently from the rigidity contrast. Geometry and boundary conditions are similar to the homogeneous thin-plate model (Figure 1b). The velocity field imposed at the base of the model is unchanged. Asymmetry is introduced by prescribing only a fault trace offset and a rigidity contrast. This contrast can be associated either with elastic parameters changes or with lateral variations of elastic plate thickness [*Chéry*, 2007]. Here we simply assume different Young's moduli for the two sides of the fault.

[16] We study in the next paragraph the asymmetric pattern of interseismic velocities observed across the eastern Altyn Tagh fault using both the half-space model and the thin-plate model.

3. Application to the Altyn Tagh Fault

3.1. Geological Settings and Slip Rate

[17] The ~2000 km-long Altyn Tagh fault (ATF) is an intra-continental, left-lateral fault marking the northern border of the Tibetan plateau, between the Tarim and the Qaidam basins (Figure 2). The ATF has been described as a major lithospheric fault accommodating part of the NS convergence between India and Asia by allowing the horizontal movement of crustal blocks and the growth of the plateau to the NE [*Meyer et al.*, 1998]. While the Qaidam is deforming in this process, the Tarim seems to be an undeformed block. Our study area is located near the old village of Aksay at ~94°E, where two parallel branches of the ATF are observed. The northern branch (NATF) is the main quaternary fault [*Mériaux et al.*, 2005]. The southern branch (SATF) is the geological fault, described as the main fault in terms of cumulative motion over longer time scale. *Mériaux et al.* [2005] estimate a 18 ± 4 mm/yr of Holocene slip rate on the fault near Aksai (~94.4°E, 39.4°N) consistent with the estimates of *Van der Woerd et al.* [2001] at Subei farther to the east (~94.9°E, 39.5°N). This rate is

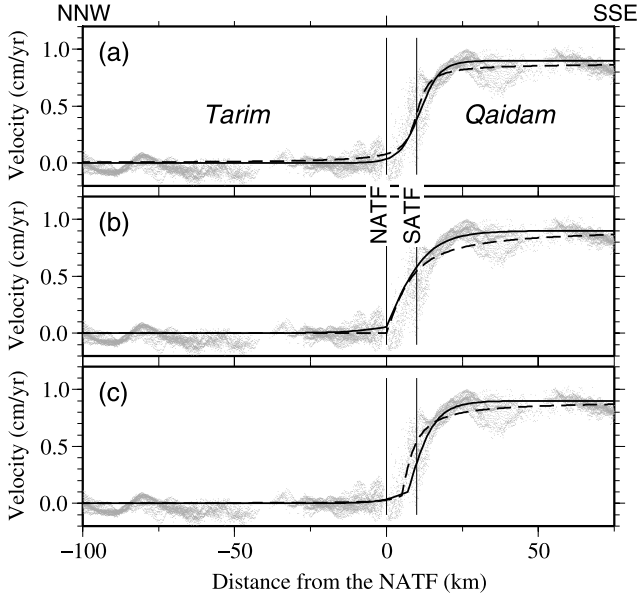

Figure 3. Interseismic velocity profile across the Altyn Tagh Fault system near Aksai. Grey dots are velocity data points in a 30 km-wide swath along profile axis (see location in Figure 2). Dashed and solid lines show calculated velocity obtained with the half-space model and the thin-plate model, respectively. The locations of northern (NATF) and southern (SATF) branches of the Altyn Tagh system are indicated by vertical lines. (a) K = 0.5 asymmetric pattern is only associated with a horizontal offset. (b) Δ = 0 km, asymmetric pattern is only due to a rigidity contrast. (c) Best-fitting model obtained with V_T = 0.9 cm/yr, D = 4 km, K = 0.9 and Δ = 5 km for the half-space model and with V_T = 0.9 cm/yr, D = 8 km, K = 0.85 and Δ = 6 km for the thin-plate model.

significantly faster than the Late Quaternary slip rate of 8–13 mm/yr obtained by *Zhang et al.* [2007] near Aksay (~94.5°E, 39.4°N).

3.2. Modeling InSAR Data With the Half-Space Model

[18] Here we use a new InSAR velocity profile from a fault-parallel velocity map to quantify interseismic strain accumulation in the Aksay region [*Lasserre et al.*, 2007]. A previous analysis of this data-set, made using a simple half-space model (equation 1) with a fault centered on the SATF, indicated a slip rate of 9–12 mm/yr and a locking depth of 0–20 km [*Lasserre et al.*, 2007]. One striking feature of the InSAR velocity profile across the fault is the clear asymmetry with respect to the NATF (Figure 2). This asymmetry is also observed in GPS measurements, which suggests that the Tarim basin behaves as a rigid block [*Zhang et al.*, 2007].

[19] We first model the velocity profile across the ATF with a half-space model, using equation 2 centered on the NATF (x = 0). We determine V_T, D, K and Δ by minimising the misfit-function χ^2 between the model velocities and the InSAR measurements. Based on the mean standard deviation of InSAR velocities we fix σ = 1 mm/yr. The best-fit model is obtained for χ^2_{best} = 0.9, V_T = 9 mm/yr, D = 4 km, K = 0.9 and Δ = 5 km (Figure 3c). V_T is well-constrained with an uncertainty of ~1 mm/yr. The fault locking depth is poorly constrained and ranges between 1 and 10 km. As expected, we observe a trade-off between the two parameters of asymmetry: K decreases from 1 to 0 when Δ increases from 0 to 17 km (Figure S3 of auxiliary material).

3.3. Modeling InSAR Data With the Thin-Plate Model

[20] The half-space model cannot explain both the observed narrow deformation zone and the far-field velocity (Figure 3). Based on the previous results, we perform an asymmetric thin-plate modeling for D' = 5–20 km and given the high number of far-field data, we fix V_T = 9 mm/yr. First, we assume a thin-plate model with a constant rigidity. The best-fit elastic thickness is 5–7 km (Figure 3a). The asymmetric pattern requires a southward offset of ~11 km, which is consistent with previous analysis of these InSAR data [*Lasserre et al.*, 2007].

[21] Next, we assume that the asymmetric pattern is only due to a lateral variation in rigidity. The location of the creeping zone is thus fixed below the NATF. On a basis of a number of simulations, the estimated K is up to 0.9 and the elastic thickness is 11–13 km (Figure 3b). This rigidity decrease between Tarim and Qaidam is in agreement with the common idea that the Tarim basin remains relatively undeformed during the Cenozoic due to the ongoing India-Eurasian collision due to the presence of a strong cratonic lithosphere.

[22] Finally, we consider that both K and Δ are free parameters. The best-fitting model suggests a rigidity contrast up to 0.85, a southward offset of 5–7 km and an elastic thickness of 7–9 km (Figure 3c). Compared to the χ^2_{best} = 0.9 obtained for the half-space model, the thin-plate approach improves the fit in particular for the high velocity gradient in the near field, with a χ^2_{best} = 0.7.

4. Conclusion

[23] We compare the conventional elastic half-space model and a thin-plate model to estimate the interseismic slip rate of strike-slip faults. We show that the HSM can lead to biased estimates of the slip rate and the fault locking depth.

[24] We apply a modified HSM and a TPM to model InSAR data across the ATF at longitude 94°. Our best TPM model implies a slip rate of 8–10 mm/yr and a locking depth of 7–9 km with a slight improvement of the χ^2 fit compare to the HSM. This result is consistent with previous estimates from GPS data at similar longitude [*Zhang et al.*, 2007].

[25] The deformation zone in the Qaidam side of the fault is remarkably wider than in the Tarim side. As proposed elsewhere by *Thatcher and Lisowski* [1987] this high InSAR velocity gradient may be associated to a weak fault zone. Our results suggest an alternative simple explanation. We interpret such a pattern as the joint effect of both a rigidity decrease from Tarim to Qaidam and a southward offset of 5–7 km from NATF to SATF. This suggests that the NATF is not the main branch of the ATF at depth and that the rigidity contrast boundary as well as the present-day creeping zone at depth are located on the SATF.

[26] **Acknowledgments.** We thank J. Chéry for the finite element code ADELI and fruitful discussions on the mechanics of interseismic loading. We acknowledge James C. Savage and Wayne Thatcher for their

thorough review, Roland Bürgmann for his comments on the initial manuscript and the Editor Aldo Zollo for his help. Figures and map were prepared using Generic Mapping Tools software [*Wessel and Smith*, 1995].

References

Chéry, J. (2007), Geodetic strain across the San Andreas Fault reflects elastic plate thickness variations (rather than fault slip rate), *Earth Planet. Sci. Lett.*, in press.

Chéry, J., M. Zoback, and R. Hassani (2001), Rheology, strain and stress of the San Andreas Fault in central and northern California: A 3-D thermo-mechanical modeling study, *J. Geophys. Res.*, *106*, 22,051–22,071.

Chinnery, M. (1961), The deformation of the ground around surface faults, *Bull. Seimol. Soc. Am.*, *51*, 355–372.

Fialko, Y. (2006), Interseismic strain accumulation and the earthquake potential on the southern San Andreas fault system, *Nature*, *441*, 968–971.

Lasserre, C., et al. (2007), Interseismic deformation across the Altyn Tagh and Haiyuan faults at the northern edge of the Tibetan plateau, measured by space geodesy, *Geophys. Res. Abstr.*, *9*, 10,102.

Le Pichon, X., N. Chamot-Rooke, C. Rangin, and A. M. C. Sengr (2003), The North Anatolian fault in the Sea of Marmara, *J. Geophys. Res.*, *108*(B4), 2179, doi:10.1029/2002JB001862.

Le Pichon, X., C. Kreemer, and N. Chamot-Rooke (2005), Asymmetry in elastic properties and the evolution of large continental strike-slip faults, *J. Geophys. Res.*, *110*, B03405, doi:10.1029/2004JB003343.

Leloup, P.-H., R. Lacassin, P. Tapponnier, Z. D. U. Schärer, L. Xiaohan, Z. Lianshang, J. Shaocheng, and P. T. Trinh (1995), The Ailao Shan–Red River shear zone (Yunnan, China), Tertiary transform boundary of Indochina, *Tectonophysics*, *251*, 3–84.

Meade, B., B. H. Hager, S. C. McClusky, R. E. Reilinger, S. Ergintav, S. Lenk, A. Barka, and H. Ozener (2002), Estimates of seismic potential in the Marmara Sea region from block models of secular deformation constrained by global positioning system measurements, *Bull. Seismol. Soc. Am.*, *92*, 208–215.

Mériaux, A., et al. (2005), The Aksay segment of the northern Altyn Tagh fault: Tectonic geomorphology, landscape evolution, and Holocene slip rate, *J. Geophys. Res.*, *110*, B04404, doi:10.1029/2004JB003210.

Meyer, B., P. Tapponnier, L. Bourjot, F. Métivier, Y. Gaudemer, G. Peltzer, G. Shunmin, and C. Zhitai (1998), Crustal thickening in Gansu-Qinghai, lithospheric mantle subduction, and oblique, strike-slip controlled growth of the Tibetan Plateau, *Geophys. J. Int.*, *135*, 1–47.

Pollitz, F., and M. Nyst (2005), A physical model for strain accumulation in the San Francisco Bay region, *Geophys. J. Int.*, *160*, 302–317.

Savage, J. C. (2006), Dislocation pileup as a representation of strain accumulation on a strike-slip fault, *J. Geophys. Res.*, *111*, B04405, doi:10.1029/2005JB004021.

Savage, J., and R. Burford (1973), Geodetic determination of relative plate motion in central California, *J. Geophys. Res.*, *78*, 832–845.

Savage, J. C., W. Gan, W. H. Prescott, and J. L. Svarc (2004), Strain accumulation across the Coast Ranges at the latitude of San Francisco, 1994–2000, *J. Geophys. Res.*, *109*, B03413, doi:10.1029/2003JB002612.

Schmalzle, G., T. Dixon, R. Malservisi, and R. Govers (2006), Strain accumulation across the Carrizo segment of the San Andreas Fault, California: Impact of laterally varying crustal properties, *J. Geophys. Res.*, *111*, B05403, doi:10.1029/2005JB003843.

Sieh, K., and P. Williams (1990), Behaviour of the southernmost San Andreas fault during the past 300 years, *J. Geophys. Res.*, *95*, 6629–6645.

Smith, B., and D. Sandwell (2003), Coulomb stress accumulation along the San Andreas Fault system, *J. Geophys. Res.*, *108*(B6), 2296, doi:10.1029/2002JB002136.

Thatcher, W., and M. Lisowski (1987), Long-term seismic potential of the San Andreas Fault southeast of San Francisco, California, *J. Geophys. Res.*, *92*, 4771–4784.

Van der Woerd, J., X. Xu, H. Li, P. Tapponnier, B. Meyer, F. Ryerson, A. Mériaux, and Z. Xu (2001), Rapid active thrusting along the northwestern range front of the Tanghe Nan Shan (western Gansu, China), *J. Geophys. Res.*, *106*, 30,475–30,504.

Vergne, J., R. Cattin, and J. Avouac (2001), On the use of dislocations to model interseismic strain and stress build-up at intracontinental thrust faults, *Geophys. J. Int.*, *147*, 155–162.

Wang, K., R. Wells, S. Mazzotti, R. D. Hyndman, and T. Sagiya (2003), A revised dislocation model of interseismic deformation of the Cascadia subduction zone, *J. Geophys. Res.*, *108*(B1), 2026, doi:10.1029/2001JB001227.

Wessel, P., and W. Smith (1995), New version of the Generic Mapping Tools released, *Eos Trans. AGU*, *76*, 329.

Wright, T., and B. P. E. Fielding (2001), Measurement of interseismic strain accumulation across the North Anatolian Fault by satellite radar interferometry, *Geophys. Res. Lett.*, *28*, 2117–2120.

Zhang, P.-Z., P. Molnar, and X. Xu (2007), Late Quaternary and present-day rates of slip along the Altyn Tagh Fault, northern margin of the Tibetan Plateau, *Tectonics*, *26*, TC5010, doi:10.1029/2006TC002014.

R. Jolivet, R. Cattin, N. Chamot-Rooke, and C. Lasserre, UMR 8538, Laboratoire de Géologie, Ecole Normale Supérieure, CNRS, F-75251 Paris, France. (romain.jolivet@ens.fr)

G. Peltzer, Department of Earth and Space Sciences, University of California, Los Angeles, CA 90095-1567, USA.